VSP

Advanced Robotics 26 (2012) 235–252

ADVANCED ROBOTICS
brill.nl/ar

Full paper

Design and Realization of a Non-Circular Cable Spool to Synthesize a Nonlinear Rotational Spring

Nicolas Schmit * **and Masafumi Okada**

Department of Mechanical Sciences and Engineering, Tokyo Institute of Technology, 2-12-1 Ookayama, Meguro-ku, Tokyo 152-8550, Japan

Received 1 April 2011; accepted 3 June 2011

Abstract

In this paper we present a cable mechanism that realizes a nonlinear rotational spring from a linear translational spring. The spring is pulled by a cable wound around a non-circular spool, which is rigidly attached to the joint. The non-circular shape of the spool induces a nonlinear relationship between its angular position and the torque created by the tension of the cable. Depending on the shape of the spool, various torque–angle relationships can be realized. We show that for a given nonlinear torque–angle relationship, there is an explicit expression (closed-form solution) of the shape of the spool that synthesizes this function. First, we present the geometry of the problem. Then, we derive the methodology to calculate the shape of the spool to synthesize a prescribed torque–angle relationship. Finally, we verify the design methodology by experiments with three different spools realizing a constant force spring, an exponential softening spring and a cubic polynomial spring. We discuss the possible sources of errors between the theoretical and experimental results.

Keywords

Nonlinear spring, nonlinear stiffness, tendon-driven mechanism, mechanical synthesis

1. Introduction

Robotic devices used for industrial processes are generally designed with very stiff links and joints to ensure accurate and high-speed positioning of the end-effector. However, in the growing field of wearable robotics, rehabilitation robotics, prosthetics and walking robots, the implementation of softness in robotic joints has become mandatory to match the requirements of shock absorption, smooth interaction with the user and energy saving. Furthermore, when designing a compliant joint as the solution to an optimization problem, we could improve the performance

* To whom correspondence should be addressed. E-mail: schmit.n.aa@m.titech.ac.jp

 DOI:10.1163/156855311X614545

of the system if we do not restrain to linear stiffness. This is because a nonlinear load–displacement function offers more design parameters than a linear function and because the space of linear functions is a subspace of the space of continuous functions.

Various applications, including (but not limited to) robotics, can benefit from nonlinear stiffness. In shock absorption devices, a hardening spring can reduce the stopping distance while a softening spring can be advisable when the structural element to be protected is unable to withstand high accelerations [1]. In manipulators, a nonlinear spring mechanism can be implemented so that the stiffness of the link drops abruptly if the external force exceeds a critical force, thus, guaranteeing the collision safety [2–4]. In an agonist–antagonist actuation mechanism, when nonlinear springs are placed in series with the actuators, the stiffness of the mechanism can be modified by a change of the co-contraction of the actuators (parametric stiffness) [5–8]. In vibration damping, nonlinear springs can be used to create a nonlinear energy sink (NES) capable of absorbing steady-state vibration energy from the main system over a relatively broad frequency range [9, 10]. Nonlinear stiffness also plays a crucial role in running/hopping robots [11]. It can improve the energy efficiency [12, 13] and the stability [14] of the motion. A detailed review of actuators taking advantage of nonlinear stiffness can be found in Ref. [15]. Finally, it is worth noticing several attempts to design simultaneously the control law and the mechanism of controlled multibody systems as the solution to an optimization problem [16, 17]. Although the methods presented in these last two papers consider only linear stiffness, we could imagine an extension to the design of nonlinear stiffness.

The implementation of nonlinear stiffness in a robotic device can be mainly achieved by two ways. The first method is to design the topology of a compliant link so that it behaves as a nonlinear spring [18, 19]. For some special class of springs, a closed-form solution of the topology of the link can be derived in order to synthesize a prescribed load–displacement function [20]. When no closed-form solution exists, a popular design method is to optimize a finite element model of the structure [21, 22]. However, in Refs [23–25], the authors proposed a new design method where the spring is modeled with splines whose parameters are optimized with a genetic algorithm. The second method to implement nonlinear stiffness is to connect a linear spring to a nonlinear transmission mechanism. This method has the benefit of using an off-the-shelf linear spring, but the drawback of the weight and size of the transmission mechanism. The design of the transmission mechanism can be achieved by optimizing the design parameters (length of links, etc.) of the mechanism to minimize the error between the prescribed and achieved load–displacement function [26]. A more accurate but complicated strategy consists in a direct computation of a part of the mechanism to synthesize exactly the prescribed load–displacement function. The nonlinearity can result from rollers moving on a curved surface [27, 28], cams [29, 30] or from a varying-radius shaft placed inside of a torsion spring [31].

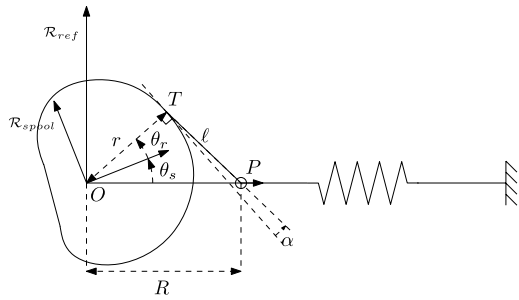

Figure 1. Transmission mechanism with a non-circular cable spool.

In this paper we present a cable mechanism that realizes a nonlinear rotational spring from a linear translational spring. The cable, connected to the linear spring, is wound around a non-circular spool as shown in Fig. 1. The non-circular shape induces a nonlinear relationship between the angular position of the spool and the torque created by the tension of the cable at the spool's axis. Depending on the non-circular shape, various nonlinear torque profiles can be realized. Compared to the mechanisms presented in Refs [26, 27, 30], the cable spool mechanism has the advantage of using very few moving parts. This not only makes the technical realization simpler, but also reduces the erroneous inertial forces that could be applied to the joint by the moving parts [29]. Indeed, the only parts not rigidly connected to the mechanical joint or the spring are the cable and the pulley, whose masses are very small. Note that a similar mechanism was proposed in Ref. [32] for weight compensation, but without deriving the closed-form solution of the shape of the spool and without experiments on the accuracy of the synthesis of the nonlinear spring.

This paper is organized as follows. Section 2 presents the mechanism, the notations and the list of assumptions. Section 3 details the methodology to derive the shape of the spool from a prescribed torque profile. We show that this problem has an exact (closed-form) solution. Section 4 presents the experimental device and the results of experiments carried out on three different shapes of spool. We discuss the possible sources of errors between the theoretical and experimental results.

2. Non-Circular Cable Spool System

We consider the mechanism shown in Fig. 1. A linear spring is connected to a cable that goes through a pulley and is wound around a non-circular spool. The spool axis is rigidly attached to the axis of the mechanical joint (not shown in Fig. 1). $\mathcal{R}_{\text{ref}}$ is the reference coordinate frame, $\mathcal{R}_{\text{spool}}$ is the coordinate frame attached to the spool, O is the axis of the spool (which is also the origin of $\mathcal{R}_{\text{ref}}$ and $\mathcal{R}_{\text{spool}}$) and θ_{s} is the angle of $\mathcal{R}_{\text{spool}}$ with respect to $\mathcal{R}_{\text{ref}}$. The pulley P is placed on the x-axis of $\mathcal{R}_{\text{ref}}$ at a distance R (>0) from O. T is the point where the cable is tangent to the spool, ℓ ($= TP$) is the length of cable between the tangency point and the pulley,

r ($= OT$) is the varying radius of the spool, θ_r is the angular position of r with respect to $\mathcal{R}_{\text{spool}}$ and α is the angle of the cable at the tangency point with respect to the perpendicular of the varying radius.

As the spool is not circular, the torque τ generated in O by the tension of the cable is a nonlinear function of the spool's angular position θ_s. The synthesis problem consists in calculating the shape of the spool to synthesize a prescribed torque–angle relationship $\tau(\theta_s)$. In the derivation of the equations of the spool's contour, we use the following simplifications:

- The stiffness of the cable is infinite (no stretching).
- The radius of the pulley is null.
- The radius of the cable is null; the real radius of the cable is considered *a posteriori* (see Section 4).

Furthermore, the origin of θ_s is defined such that $0 \leqslant \theta_s \leqslant \theta_{s,\max}$.

3. Synthesis of the Non-Circular Spool

3.1. Geometry of the Proposed System

To calculate the shape of the spool, we first translate the prescribed torque–angle relationship into a kinematic relationship. From the principe of virtual work:

$$\tau(\theta_s)\,\mathrm{d}\theta_s = kq\,\mathrm{d}q, \tag{1}$$

where q is the displacement of the linear spring with respect to its natural length and k is the spring constant. Since the tension of the cable must be strictly positive, we assume that $\tau(\theta_s) > 0$ and $q > 0$. From (1), we define the function J as:

$$J(\theta_s) = \frac{\mathrm{d}q}{\mathrm{d}\theta_s} = \frac{1}{k}\frac{\tau(\theta_s)}{q}. \tag{2}$$

We integrate (1) to obtain the expression of q:

$$\tau(\theta_s)\,\mathrm{d}\theta_s = \frac{1}{2}k\,\mathrm{d}(q^2) \tag{3}$$

$$\frac{2}{k}\int_0^{\theta_s} \tau(u)\,\mathrm{d}u = q^2 - q_0^2 \tag{4}$$

$$q = \sqrt{\frac{2}{k}\int_0^{\theta_s} \tau(u)\,\mathrm{d}u + q_0^2}, \tag{5}$$

where q_0 is the displacement of the spring when $\theta_s = 0$. Substituting (5) in (2), we obtain:

$$J(\theta_s) = \frac{\tau(\theta_s)}{\sqrt{2k\int_0^{\theta_s} \tau(u)\,\mathrm{d}u + (kq_0)^2}}. \tag{6}$$

$J(\theta_s)$ defines the kinematic input/output relationship that the spool must achieve to synthesize the torque–angle relationship $\tau(\theta_s)$. $J(\theta_s)$ can be seen as the translation of a torque synthesis problem into a kinematic synthesis problem.

As shown in Fig. 1, the spool's contour is defined in polar coordinates by the relationship $r(\theta_r)$. Considering that the problem is parameterized by θ_s, we need to determine two independent equations between r, θ_r and θ_s to solve the problem.

3.2. Tangency Condition

We consider the displacement of the tangency point T for a small variation of θ_r, as shown in Fig. 2. We note δa the distance between $T(\theta_r)$ and $T(\theta_r + \delta\theta_r)$. Using the law of cosines, we obtain:

$$(\delta a)^2 = (r(\theta_r))^2 + (r(\theta_r + \delta\theta_r))^2 - 2r(\theta_r)r(\theta_r + \delta\theta_r)\cos(\delta\theta_r) \tag{7}$$

$$(r(\theta_r))^2 = (r(\theta_r + \delta\theta_r))^2 + (\delta a)^2 - 2r(\theta_r + \delta\theta_r)\delta a\cos\varphi. \tag{8}$$

We substitute (7) in (8) then calculate the Taylor expansion in $\delta\theta_r$:

$$2r\left(\frac{\mathrm{d}r}{\mathrm{d}\theta_r} - \sqrt{\left(\frac{\mathrm{d}r}{\mathrm{d}\theta_r}\right)^2 + r^2}\cos\varphi\right) + \mathcal{O}(\delta\theta_r) = 0. \tag{9}$$

By taking the limit of $\delta\theta_r$ in 0, we obtain:

$$\cos\varphi_0 = \frac{\frac{\mathrm{d}r}{\mathrm{d}\theta_r}}{\sqrt{(\frac{\mathrm{d}r}{\mathrm{d}\theta_r})^2 + r^2}}, \tag{10}$$

where $\varphi_0 = \lim_{\delta\theta_r \to 0} \varphi$. Finally, substituting the relation $\varphi_0 = \frac{\pi}{2} + \alpha$ in (10), we obtain:

$$\tan\alpha = -\frac{1}{r}\frac{\mathrm{d}r}{\mathrm{d}\theta_r}. \tag{11}$$

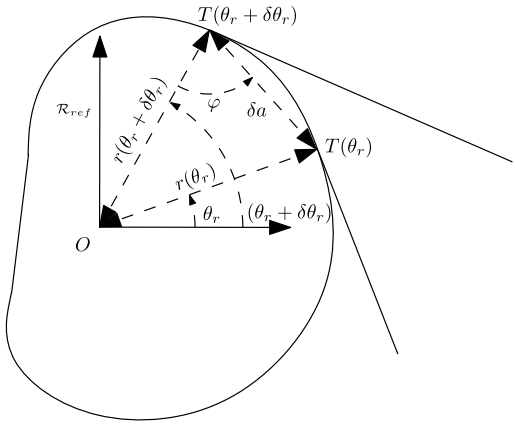

Figure 2. Displacement of the tangency point.

Equation (11) is called the tangency equation. The angle α can be calculated using the formula given in the Appendix.

3.3. Conservation of the Total Length of Cable

We note ℓ_{spool} the length of cable wound around the spool, ℓ_{spring} the length of cable from the pulley to the spring and L the total length of cable. Since the total length of cable is constant:

$$\frac{\mathrm{d}L}{\mathrm{d}\theta_{\text{s}}} = \frac{\mathrm{d}\ell_{\text{spool}}}{\mathrm{d}\theta_{\text{s}}} + \frac{\mathrm{d}\ell}{\mathrm{d}\theta_{\text{s}}} + \frac{\mathrm{d}\ell_{\text{spring}}}{\mathrm{d}\theta_{\text{s}}} = 0. \tag{12}$$

We now detail the calculation of the three terms of the right-hand side of (12).

3.3.1. First Term

We write $\frac{\mathrm{d}\ell_{\text{spool}}}{\mathrm{d}\theta_{\text{s}}}$ as:

$$\frac{\mathrm{d}\ell_{\text{spool}}}{\mathrm{d}\theta_{\text{s}}} = \frac{\mathrm{d}\ell_{\text{spool}}}{\mathrm{d}\theta_r}\frac{\mathrm{d}\theta_r}{\mathrm{d}\theta_{\text{s}}}. \tag{13}$$

We calculate the second-order Taylor expansion in $\delta\theta_r$ of (7) and remove the term $\frac{\mathrm{d}r}{\mathrm{d}\theta_r}$ using (11). We obtain:

$$(\delta a)^2 = \frac{r^2}{\cos^2(\alpha)}(\delta\theta_r)^2 + \mathcal{O}\big((\delta\theta_r)^3\big). \tag{14}$$

From (14), we calculate $\frac{\mathrm{d}\ell_{\text{spool}}}{\mathrm{d}\theta_r}$ as:

$$\frac{\mathrm{d}\ell_{\text{spool}}}{\mathrm{d}\theta_r} = -\lim_{\delta\theta_r\to 0}\frac{\delta a}{\delta\theta_r} = -\frac{r}{\cos\alpha}. \tag{15}$$

Thus, the first term of the right-hand side of (12) is:

$$\frac{\mathrm{d}\ell_{\text{spool}}}{\mathrm{d}\theta_{\text{s}}} = -\frac{r}{\cos\alpha}\frac{\mathrm{d}\theta_r}{\mathrm{d}\theta_{\text{s}}}. \tag{16}$$

3.3.2. Second Term

Using the law of cosines in Fig. 1, ℓ is calculated as:

$$\ell = \sqrt{R^2 + r^2 - 2Rr\cos(\theta_r + \theta_{\text{s}})}. \tag{17}$$

The total derivative of ℓ with respect to θ_{s} is represented by:

$$\begin{aligned}\frac{\mathrm{d}\ell}{\mathrm{d}\theta_{\text{s}}} &= \frac{\partial\ell}{\partial\theta_r}\frac{\mathrm{d}\theta_r}{\mathrm{d}\theta_{\text{s}}} + \frac{\partial\ell}{\partial r}\frac{\mathrm{d}r}{\mathrm{d}\theta_{\text{s}}} + \frac{\partial\ell}{\partial\theta_{\text{s}}} \\ &= \left(\frac{\partial l}{\partial\theta_r} + \frac{\partial l}{\partial r}\frac{\mathrm{d}r}{\mathrm{d}\theta_r}\right)\frac{\mathrm{d}\theta_r}{\mathrm{d}\theta_{\text{s}}} + \frac{\partial\ell}{\partial\theta_{\text{s}}}.\end{aligned} \tag{18}$$

From (17), we calculate the partial derivatives of ℓ with respect to r, θ_r and θ_{s}:

$$\frac{\partial\ell}{\partial r} = \frac{r - R\cos(\theta_r + \theta_{\text{s}})}{\ell} \tag{19}$$

$$\frac{\partial \ell}{\partial \theta_r} = \frac{Rr\sin(\theta_r + \theta_s)}{\ell} \tag{20}$$

$$\frac{\partial \ell}{\partial \theta_s} = \frac{Rr\sin(\theta_r + \theta_s)}{\ell}. \tag{21}$$

Substituting (19)–(21) in (18), and using (11) to remove the term $\frac{dr}{d\theta_r}$, we obtain:

$$\frac{d\ell}{d\theta_s} = \frac{r}{\cos\alpha}\frac{d\theta_r}{d\theta_s} + \frac{Rr}{\ell}\sin(\theta_r + \theta_s). \tag{22}$$

3.3.3. Third Term

Since the pulley and the anchor of the spring are fixed, the length $\ell_{spring} + q$ is constant. Thus, we obtain from (6):

$$\frac{d\ell_{spring}}{d\theta_s} = -\frac{dq}{d\theta_s} = -J(\theta_s). \tag{23}$$

3.4. Calculation of the Explicit Solution

By substituting (16), (22) and (23) in (12), we obtain:

$$\frac{Rr}{\ell}\sin(\theta_r + \theta_s) = J(\theta_s). \tag{24}$$

This is a first constraint relationship between r, θ_r and θ_s. We now substitute (17) in (24), take the square of this equation and write it as:

$$\mathcal{G} = \frac{R^2 r^2 \sin^2(\theta_r + \theta_s)}{R^2 + r^2 - 2Rr\cos(\theta_r + \theta_s)} = J^2(\theta_s). \tag{25}$$

Using (11) to remove the term $\frac{dr}{d\theta_r}$, the derivative of this equation with respect to θ_s is:

$$\frac{d\mathcal{G}}{d\theta_s} = \left(\frac{\partial \mathcal{G}}{\partial \theta_r} - r\tan\alpha\frac{\partial \mathcal{G}}{\partial r}\right)\frac{d\theta_r}{d\theta_s} + \frac{\partial \mathcal{G}}{\partial \theta_s} = 2J(\theta_s)J'(\theta_s), \tag{26}$$

where $J'(\theta_s)$ stands for $\frac{dJ(\theta_s)}{d\theta_s}$. We give the partial derivatives of $\mathcal{G}$:

$$\frac{\partial \mathcal{G}}{\partial r} = 2\frac{R^3 r}{\ell^4}\sin^2(\theta_r + \theta_s)(R - r\cos(\theta_r + \theta_s)) \tag{27}$$

$$\frac{\partial \mathcal{G}}{\partial \theta_r} = 2\frac{R^2 r^2}{\ell^4}\sin(\theta_r + \theta_s)\left[\cos(\theta_r + \theta_s)(R^2 + r^2) - \left(1 + \cos^2(\theta_r + \theta_s)\right)Rr\right] \tag{28}$$

$$\frac{\partial \mathcal{G}}{\partial \theta_s} = 2\frac{R^2 r^2}{\ell^4}\sin(\theta_r + \theta_s)\left[\cos(\theta_r + \theta_s)(R^2 + r^2) - \left(1 + \cos^2(\theta_r + \theta_s)\right)Rr\right]. \tag{29}$$

Equation (26) should lead to a differential equation on $\frac{d\theta_r}{d\theta_s}$. However, the value of $(\frac{\partial \mathcal{G}}{\partial \theta_r} - r\tan\alpha\frac{\partial \mathcal{G}}{\partial r})$ is exactly zero no matter the values of r, θ_r and θ_s. Thus, (26) is reduced to:

$$\frac{d\mathcal{G}}{d\theta_s} = \frac{\partial \mathcal{G}}{\partial \theta_s} = 2J(\theta_s)J'(\theta_s). \tag{30}$$

Substituting (29) in the above equation, we obtain:

$$\frac{R^2r^2}{\ell^4}\sin(\theta_r+\theta_s)\cdot\left[\cos(\theta_r+\theta_s)(R^2+r^2)-\left(1+\cos^2(\theta_r+\theta_s)\right)Rr\right] = J(\theta_s)J'(\theta_s). \tag{31}$$

This is a second constraint relationship between r, θ_r and θ_s. For a given set of θ_s, the spool contour is defined by the set of (r,θ_r) solution of the system (24) and (31).

We now solve the system (24) and (31) to obtain the explicit solution of the spool contour. After substituting ℓ using (17), (24) is equivalent to:

$$R^2r^2X^2-2RrJ^2X+(R^2+r^2)J^2-R^2r^2=0, \tag{32}$$

where $X=\cos(\theta_r+\theta_s)$. Note that to clarify the equations, we use the simplified notation J instead of $J(\theta_s)$. Assuming that $0<J\leqslant r<R$, the roots of (32) are:

$$X=\frac{RrJ^2\pm\sqrt{\Delta}}{R^2r^2}$$
$$\Delta=R^2r^2(R^2-J^2)(r^2-J^2). \tag{33}$$

Thus, θ_r is obtained as:

$$\theta_r=-\theta_s+\arccos\left(\frac{J^2\pm\sqrt{(r^2-J^2)(R^2-J^2)}}{Rr}\right). \tag{34}$$

The $\pm$ symbol in (34) comes from the two distinct roots of (32). We will show later that this symbol must be chosen equal to $\mathrm{sgn}(J')$.

After substituting (17) and (34), (31) is equivalent to:

$$\frac{R^2r^2\sqrt{1-(\frac{1}{Rr}(J^2\pm\Lambda))^2}}{(R^2+r^2-2Rr(\frac{1}{Rr}(J^2\pm\Lambda)))^2}\cdot\left(r\left(\frac{1}{Rr}(J^2\pm\Lambda)\right)-R\right)\cdot\left(r-R\left(\frac{1}{Rr}(J^2\pm\Lambda)\right)\right)=JJ', \tag{35}$$

where $\Lambda=\sqrt{(r^2-J^2)(R^2-J^2)}$. After simplifications, this equation is equivalent to

$$(R^2+r^2-2(J^2\pm\Lambda))^{-3/2}[-(J^2\pm\Lambda)^2+(r^2+R^2)(J^2\pm\Lambda)-R^2r^2] = J'. \tag{36}$$

We now define $r^*=\sqrt{r^2-J^2}$ and $R^*=\sqrt{R^2-J^2}$. Equation (36) is equivalent to:

$$\pm\frac{r^*R^*}{R^*\mp r^*}=J'. \tag{37}$$

Since we imposed the condition $r < R$, $(R^* \mp r^*)$ is positive. Thus, the $\pm$ symbol in (34)–(37) must be chosen equal to $\mathrm{sgn}(J')$. From (37), the explicit solution of r is obtained as:

$$r = \sqrt{J^2(\theta_s) + \frac{J'^2(\theta_s)(R^2 - J^2(\theta_s))}{(J'(\theta_s) + \sqrt{R^2 - J^2(\theta_s)})^2}}. \tag{38}$$

We note that this last equation does not depend on $\mathrm{sgn}(J')$. The system (34) and (38) defines the unique explicit solution of the spool contour for a given function $J(\theta_s)$. For a given set of θ_s, we first use (6) to calculate J, then we use (38) to calculate the set of r and finally we use (34) to calculate the set of θ_r. An important remark is that a necessary condition so that a solution exists is $J \leqslant r$. Under this condition, the radius of the spool verifies the relationship $J(\theta_s) \leqslant r(\theta_s) < R$. Furthermore, since the tension in the cable must stay positive, the objective torque profile $\tau(\theta_s)$ must be strictly positive.

3.5. Example of Design

To illustrate the design methodology, we calculated three different spools realizing a constant force spring, an exponential softening spring and a cubic polynomial spring. The shape of the spools is shown in Figs 3a–5a; the prescribed torque–angle relationship is shown in Figs 3b–5b; the varying radius r is shown in Figs 3c–5c; and the torsional stiffness of the mechanism is shown in Figs 3d–5d. The spools are shown at the angular position $\theta_s = 0$ and rotate counterclockwise when θ_s increases. The angular displacement range is $[0°, 270°]$ (identical for all three spools). As shown in Fig. 5, although the spring is always pulled when the spool rotates counterclockwise, it is possible to realize a torque profile with a locally negative stiffness. This is achieved by a sudden drop in the radius r.

3.6. Choice of Design Parameters

In the derivation of the equations of the spool (J (6), r (38), θ_r (34)), we introduced three design parameters: the spring constant k, the spring preloading (kq_0) and the location of the pulley R. Since the prescribed torque–angle relationship is embedded in (6), a change of one or several design parameters results in a different spool shape, but does not affect the torque–angle relationship of the mechanism. We illustrate this property with a simple example: for each set of design parameters shown in Table 1, we calculated the spool synthesizing the torque profile shown in Fig. 5b. The spools are shown in Fig. 6.

The set $\{k, q_0, R\}$ can be chosen to optimize a design criterion, such as minimizing the size of the mechanism. However, calculating the set $\{k, q_0, R\}$ that optimizes a given design criterion is a complicated optimization problem because the equations of the spool are highly nonlinear, and because the design has to satisfy complicated geometric constraints to ensure that the contour is convex and without loops. In this paper, we will not say anything further about the optimization of the design parameters as this will addressed in a future publication.

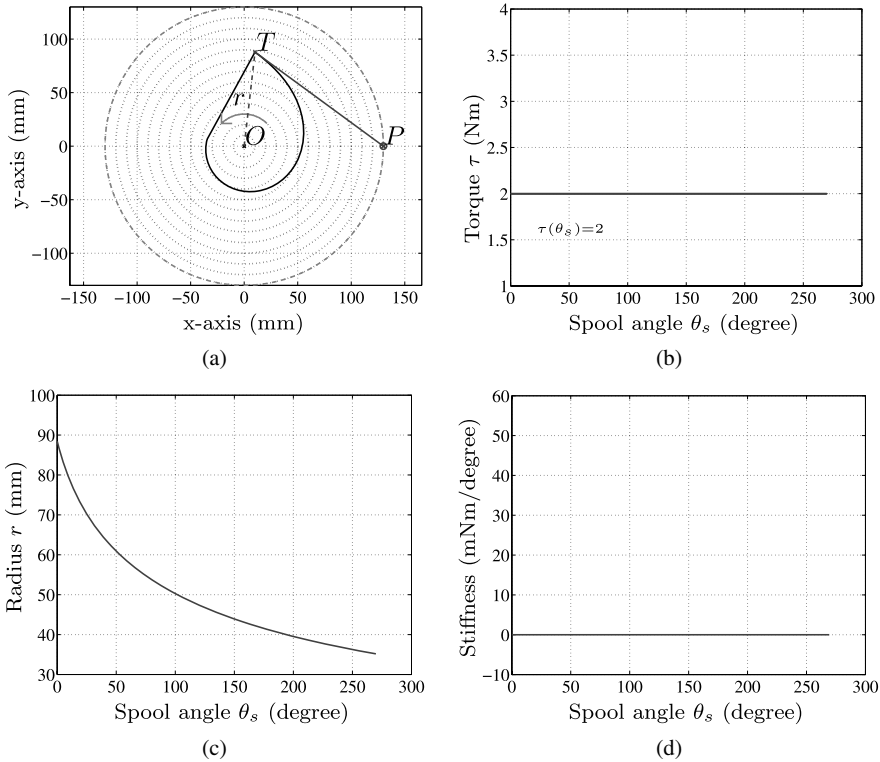

Figure 3. Constant force spring. (a) Spool; (b) torque profile; (c) varying radius; (d) torsional stiffness.

4. Experiments

4.1. Description of the Experimental Device

The experimental device is shown in Fig. 7: from the right to the left: the spool, a torque sensor, a harmonic gear and a handle. Thanks to the high reduction ratio of the harmonic gear (1:50), the spool can be rotated easily by the experimentator using the handle. We use a scale printed on the handle to measure the position of the spool. In this experiment, we neglect the angular error due to the twist of the kinematic chain (gear + couplings + sensor). Indeed, the torsional stiffness of the kinematic chain from the handle to the spool is 313 Nm/rad and since in our experiments the torque at the spool's axis does not exceed 4 Nm, the maximum angular error is 0.732° (see Table 2 for the stiffness of the transmission components). The experiments are carried out with the three spools presented in Section 3.5. The spools are cut in an 8-mm-thick aluminum board using a wire-cut machine tool. In order to take into account the thickness of the wire, we removed 0.4 mm from the theoretical radius r. The cable is a steel wire whose diameter is 0.8 mm. We assume the stretching of the cable to be negligible. The linear spring, which consists of three identical springs in series, has a stiffness constant of 137 N/m. The pulley has a diameter of 6 mm and is located 130 mm from the axis of the spool.

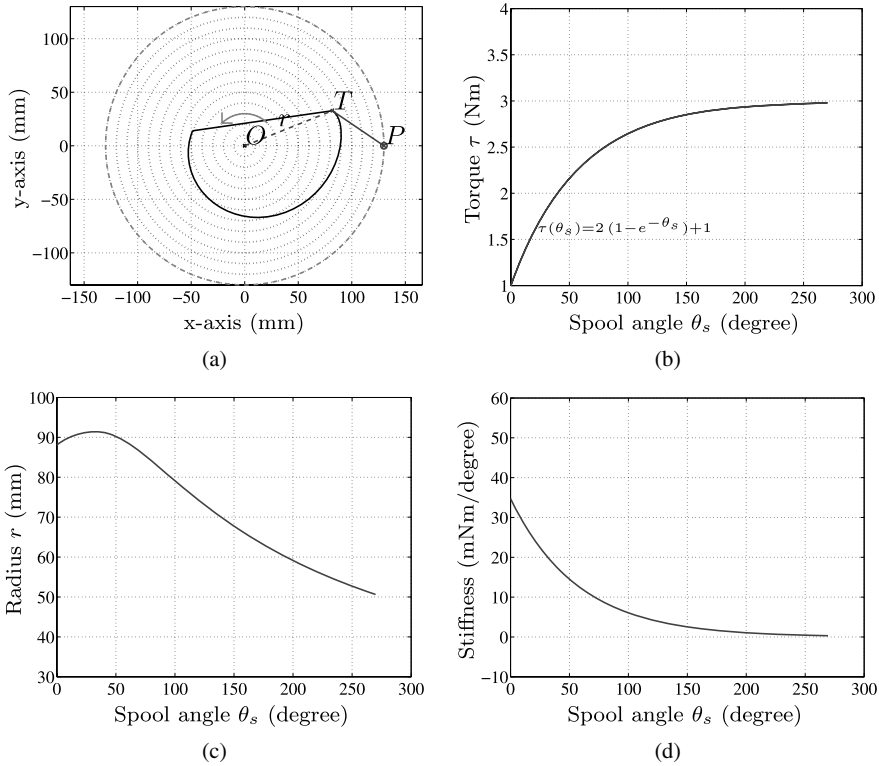

Figure 4. Exponential softening spring. (a) Spool; (b) torque profile; (c) varying radius; (d) torsional stiffness.

4.2. Experimental Results

The comparison of the theoretical (solid line) and experimental (x-mark line) torque–angle relationship is shown in Figs 8a–10a. The experiments consisted in increasing θ_s from 0 to 270°, then decreasing θ_s back to 0°. We subtracted from the experimental data the gravity moment due to the weight of the spool (calculated as a function of θ_s using the mass and location of the center of mass (COM) given in Table 3 (the coordinates of the COM where calculated numerically by CAD software)). The relative torque error is shown in Figs 8b–10b. The average torque error for the three spools is about 1.5%. The error consists mainly in a hysteresis effect (higher torque when increasing θ_s) that might be caused by friction in the ball bearings. This can be easily seen in Fig. 10b. However, in Fig. 9b the error seems to be correlated with the position of the spool. A possible explanation is a small error in the preloading of the spring (kq_0), which affects the load–displacement function. To estimate the influence of the preloading on the synthesized torque profile, we rewrite (2) as:

$$\tau(\theta_s) = F(q)J(\theta_s), \tag{39}$$

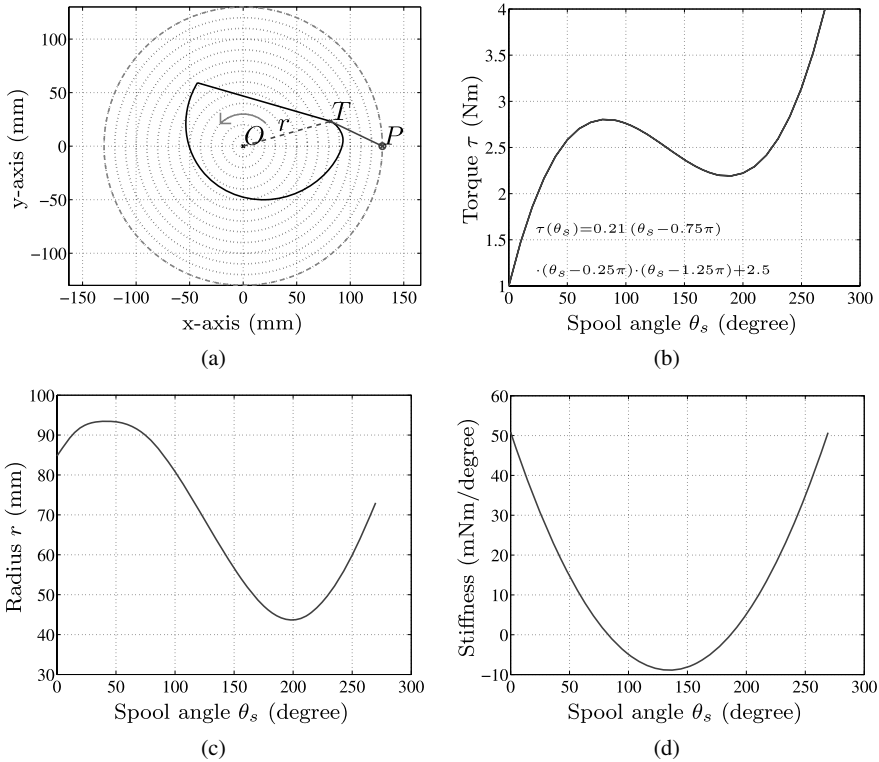

Figure 5. Cubic polynomial spring. (a) Spool; (b) torque profile; (c) varying radius; (d) torsional stiffness.

where $F(q) = kq$ is the restoring force of the linear spring. For a given design, J is fixed. (By definition $J(\theta_s) = \frac{dq}{d\theta_s}$, which is a kinematic relationship independent of the preloading.) Thus, from (39), we can easily derive the sensitivity of the torque profile to an error in the tension of the spring:

$$\left.\frac{\partial \tau}{\partial F}\right|_J = J(\theta_s). \tag{40}$$

A shift in the preloading of the spring δF will shift the torque profile by $\delta\tau = J(\theta_s)\delta F$. The sensitivity depends on the magnitude of $J(\theta_s)$ at a given spool angle θ_s. The plot of $J(\theta_s)$ (calculated using (6)) for the three designs is shown in Fig. 11.

With the experimental device presented in this paper, it is not possible to finely tune the preloading of the spring. In future designs, we plan to add a screw to tune the preloading in order to increase the accuracy of the synthesized torque profile.

5. Conclusions

In this paper, we proposed a cable mechanism based on a non-circular spool that synthesizes a nonlinear rotational spring from a linear spring. We showed that for a

Table 1.
Design parameters

k (N/m)	q_0 (mm)	R (mm)
137	130	130
170	140	100
205	170	70
1233	127	24

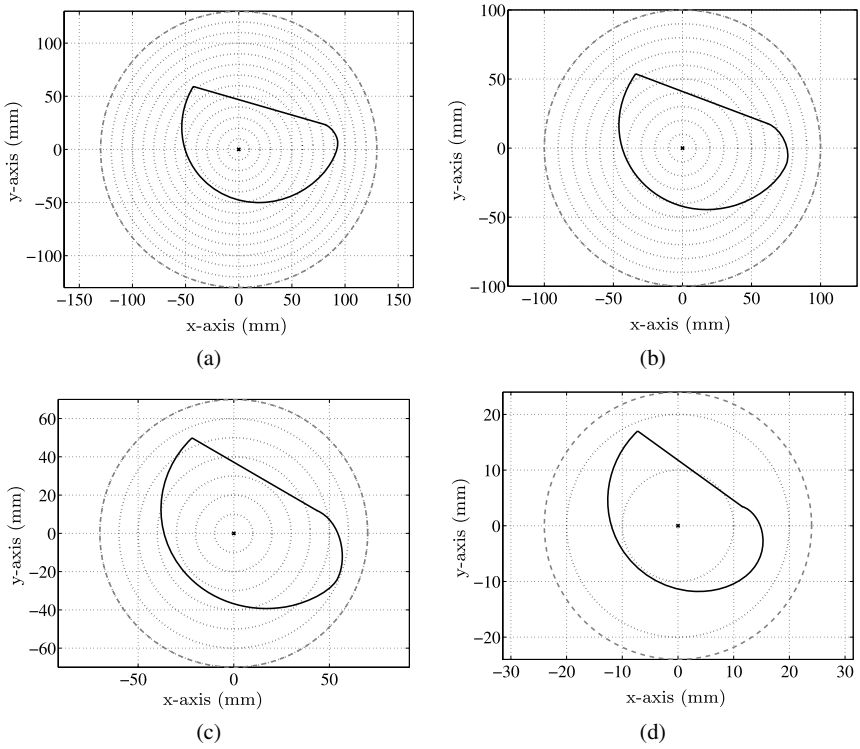

Figure 6. Spools calculated with the same torque–angle relationship, but different design parameters. (a) $R = 130$ mm; (b) $R = 100$ mm; (c) $R = 70$ mm; (d) $R = 24$ mm.

prescribed torque–angle relationship $\tau(\theta_s)$, there is an explicit expression (closed-form solution) of the shape of the spool that synthesizes this function. We derived the equations of the spool, then verified the design methodology by experiments with three different spools realizing a constant force spring, an exponential softening spring and a cubic polynomial spring. The experiments showed that the prescribed torque–angle relationships where achieved with an average accuracy of 1.5%. This mechanism has the advantage of using very few moving parts, which

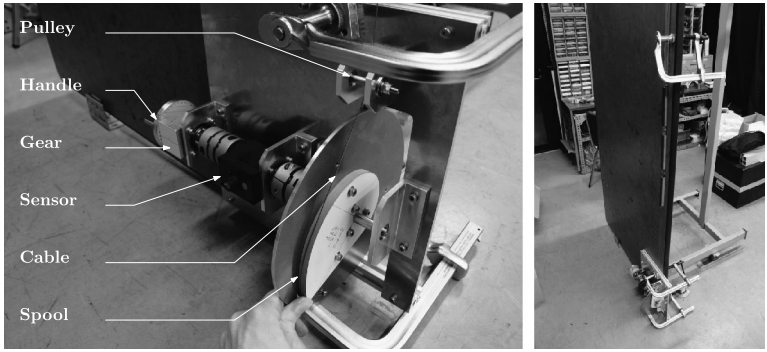

Figure 7. Experimental device.

Table 2.
Stiffness of the kinematic chain

Transmission component	Stiffness (Nm/rad)
Torque sensor	498
Coupling (×2)	1.90×10^3
Harmonic gear (1:50)	7.41×10^3

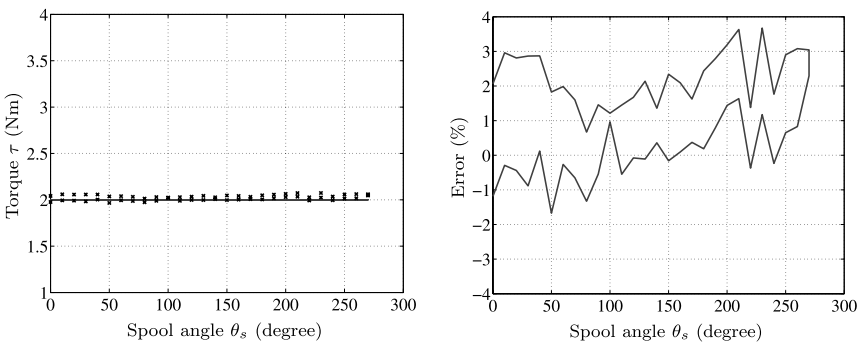

Figure 8. Constant force spring. (a) Torque *vs*. spool's angular position. (b) Relative torque error.

makes it easy to manufacture and reduces the erroneous inertial forces that could be applied to the joint by moving parts.

Future work will include the development of a compact nonlinear spring unit that could fit in the ankle joint of a walking robot. We also plain to develop an antagonistic spring mechanism that could synthesize a torque profile with both positive and negative magnitude.

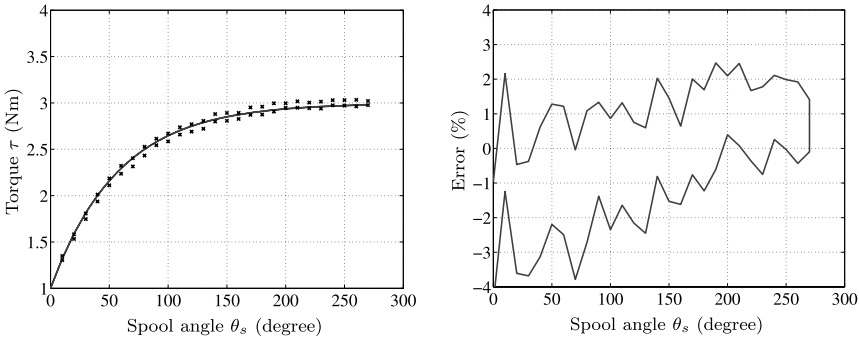

(a) (b)

Figure 9. Exponential softening spring. (a) Torque *vs*. spool's angular position. (b) Relative torque error.

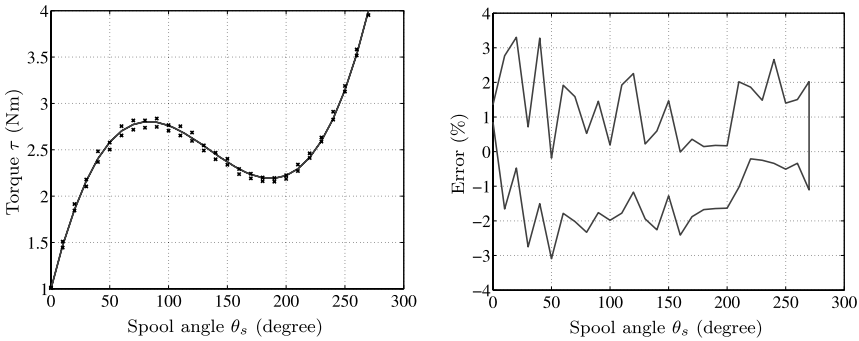

(a) (b)

Figure 10. Cubic polynomial spring (a) Torque *vs*. spool's angular position. (b) Relative torque error.

Table 3.
Inertial characteristics of the spools

Spool no.	Mass (g)	Coordinates of the COM (mm)
1	172	(11.3, 15.6)
2	226	(19.8, −15.4)
3	233	(14.1, 1.65)

Acknowledgements

This research is supported by the Research on Macro/Micro Modeling of Human Behavior in the Swarm and its Control under the Core Research for Evolutional Science and Technology (CREST) Program (research area: Advanced Integrated Sensing Technologies), Japan Science and Technology Agency (JST).

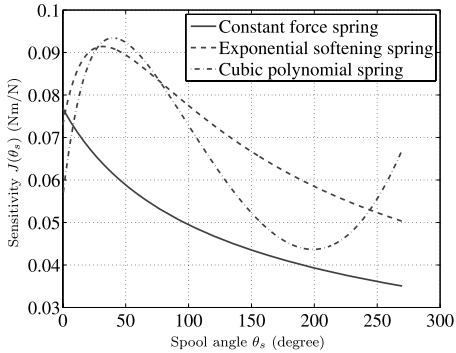

Figure 11. Sensitivity of the torque profile to a error in the preloading of the spring.

References

1. E. Suhir, Shock protection with a nonlinear spring, *IEEE Trans. Comp. Pack. Manufact. Technol.* **18**, 430–437 (1995).
2. J.-J. Park, B.-S. Kim, J.-B. Song and H.-S. Kim, Safe link mechanism based on passive compliance for safe human–robot collision, in: *Proc. IEEE Int. Conf. on Robotics and Automation*, Rome, pp. 1152–1157 (2007).
3. J.-J. Park, H.-S. Kim and J.-B. Song, Safe robot arm with safe joint mechanism using nonlinear spring system for collision safety, in: *Proc. IEEE Int. Conf. on Robotics and Automation*, Kobe, pp. 3371–3376 (2009).
4. J.-J. Park, Y.-J. Lee, J.-B. Song and H.-S. Kim, Safe joint mechanism based on nonlinear stiffness for safe human–robot collision, in: *Proc. IEEE Int. Conf. on Robotics and Automation*, Pasadena, CA, pp. 2177–2182 (2008).
5. K. F. Laurin-Kovitz, J. E. Colgate and S. D. R. Carnes, Design of components for programmable passive impedance, in: *Proc. IEEE Int. Conf. on Robotics and Automation*, Sacramento, CA, Vol. 2, pp. 1476–1481 (1991).
6. A. Katz, The design and application of a nonlinear series compliance actuator for use in robotic arms, *MA Thesis*, Department of Mechanical Engineering, MIT (1999).
7. A. Bicchi and G. Tonietti, Design, realization and control of soft robot arms for intrinsically safe interaction with humans, *Technical Report*, Centro Interdipartimentale di Ricerca 'E. Piaggio', Universita di Pisa (2002).
8. K. Koganezawa, Y. Watanabe and N. Shimizu, Antagonistic muscle-like actuator and its application to multi-d.o.f. forearm prosthesis, *Adv. Robotics* **12**, 771–789 (1997).
9. X. Jiang, D. M. McFarland, L. A. Bergman and A. F. Vakakis, Steady state passive nonlinear energy pumping in coupled oscillators: theoretical and experimental results, *Nonlinear Dyn.* **33**, 87–102 (2003).
10. D. M. McFarland, L. A. Bergman and A. F. Vakakis, Experimental study of non-linear energy pumping occurring at a single fast frequency, *Int. J. Non-Linear Mech.* **40**, 891–899 (2005).
11. R. N. McAlexander, Three uses for springs in legged locomotion, *Int. J. Robotics Res.* **9**, 53–61 (1990).
12. J. Yamaguchi and A. Takanishi, Design of biped walking robots having antagonistic driven joints using nonlinear spring mechanism, in: *Proc. IEEE/RSJ Int. Conf. on Intelligent Robots and Systems*, Grenoble, Vol. 1, pp. 251–259 (1997).

13. J. Yamaguchi, D. Nishino and A. Takanishi, Realization of dynamic biped walking varying joint stiffness using antagonistic driven joints, in: *Proc. IEEE Int. Conf. on Robotics and Automation*, Leuven, Vol. 3, pp. 2022–2029 (1998).
14. D. Owaki and A. Ishiguro, Enhancing stability of a passive dynamic running biped by exploiting a nonlinear spring, in: *Proc. IEEE/RSJ Int. Conf. on Intelligent Robots and Systems*, Beijing, pp. 4923–4928 (2006).
15. R. Ham, T. Sugar, B. Vanderborght, K. Hollander and D. Lefeber, Compliant actuator designs, *IEEE Robotics Automat. Mag.* **16**, 81–94 (2009).
16. K. D. Mombaur, R. W. Longman, H. G. Bock and J. P. Schloder, Open-loop stable running, *Robotica* **23**, 21–33 (2005).
17. V. E. Berbyuk and A. E. Bostrom, Optimization problems of controlled multibody systems having spring–damper actuators, *Int. Appl. Mech.* **37**, 935–940 (2001).
18. M. Okada, Y. Nakamura and S. Ban, Design of programmable passive compliance shoulder mechanism, in: *Proc. IEEE Int. Conf. on Robotics and Automation*, Seoul, Vol. 1, pp. 348–353 (2001).
19. M. Okada and S. Kino, Torque transmission mechanism with nonlinear passive stiffness using mechanical singularity, in: *Proc. IEEE Int. Conf. on Robotics and Automation*, Pasadena, CA, pp. 1735–1740 (2008).
20. C. English and D. Russell, Implementation of variable joint stiffness through antagonistic actuation using rolamite springs, *Mech. Mach. Theory* **34**, 27–40 (1999).
21. T. Buhl, C. B. W. Pedersen and O. Sigmund, Stiffness design of geometrically nonlinear structures using topology optimization, *Struct. Multidisciplin. Optimizat.* **19**, 93–104 (2000).
22. T. E. Bruns and D. A. Tortorelli, Topology optimization of non-linear elastic structures and compliant mechanisms, *Comp. Methods Appl. Mech. Eng.* **190**, 3443–3459 (2001).
23. C. Vehar Jutte, Generalized synthesis methodology of nonlinear springs for prescribed load–displacement functions, *PhD thesis*, University of Michigan (2008).
24. C. Vehar Jutte and S. Kota, Design of single, multiple, and scaled nonlinear springs for prescribed nonlinear responses, *J. Mech. Des.* **132**, 011003 (2010).
25. C. Vehar Jutte and S. Kota, Design of nonlinear springs for prescribed load–displacement functions, *J. Mech. Des.* **130**, 081403 (2008).
26. M. Okada and J. Takeishi, Kineto-static mechanical synthesis for nonlinear property design of passive stiffness using closed kinematic chain, in: *Proc. IEEE/RSJ Int. Conf. on Intelligent Robots and Systems*, Taipei, pp. 4213–4218 (2010).
27. S. A. Migliore, E. A. Brown and S. P. DeWeerth, Biologically inspired joint stiffness control, in: *Proc. IEEE Int. Conf. on Robotics and Automation*, Barcelona, pp. 4508–4513 (2005).
28. S. Wolf and G. Hirzinger, A new variable stiffness design: matching requirements of the next robot generation, in: *Proc. IEEE Int. Conf. on Robotics and Automation*, Pasadena, CA, pp. 1741–1746 (2008).
29. S. A. Migliore, E. A. Brown and S. P. DeWeerth, Novel nonlinear elastic actuators for passively controlling robotic joint compliance, *J. Mech. Des.* **129**, 406–412 (2007).
30. J. W. Hurst, J. Chestnutt and A. Rizzi, An actuator with mechanically adjustable series compliance, *Technical Report CMU-RI-TR-04-24*, Robotics Institute, Carnegie Mellon University (2004).
31. K. Koganezawa, Mechanical stiffness control for antagonistically driven joints, in: *Proc. IEEE/RSJ Int. Conf. on Intelligent Robots and Systems*, Edmonton, pp. 1544–1551 (2005).
32. G. Endo, H. Yamada, A. Yajima, M. Ogata and S. Hirose, A passive weight compensation mechanism with a non-circular pulley and a spring, in: *Proc. IEEE Int. Conf. on Robotics and Automation*, Anchorage, AK, pp. 3843–3848 (2010).

About the Authors

Nicolas Schmit graduated from the Ecole Polytechnique, Paris, and from the Institut Superieur de l'Aeronautique et de l'Espace (Supaero), Toulouse (France), in 2009. He is currently pursuing the PhD degree in Mechanical Engineering at Tokyo Institute of Technology, Tokyo. His dissertation research is on the optimal design of nonlinear stiffness of robotic mechanisms. He did his graduation internship at Thales Alenia Space's Research Department, Cannes (France), from April 2009 to September 2009. His research was on the robust control of telecom satellites subject to unstable fuel sloshing phenomena. He currently holds a fellowship from the Japanese government (Monbukagakusho: MEXT).

Masafumi Okada received his ME and PhD degrees in Applied System Science from Kyoto University, in 1994 and 1996, respectively. In 1997, he joined the Department of Mechano-Informatics, University of Tokyo, and he is currently an Associate Professor in the Department of Mechanical Sciences and Engineering, Tokyo Institute of Technology. His interests include an attractor-based robot control, mechanical design with nonlinear stiffness and amenity design for human environments.

Appendix: Calculation of α

These expressions can be obtained easily by application of the law of cosines to the triangle *POT* in Fig. 1:

$$\cos\alpha = \frac{R}{\ell}\sin(\theta_r + \theta_s) \tag{A.1}$$

$$\sin\alpha = \frac{R}{\ell}\cos(\theta_r + \theta_s) - \frac{r}{\ell} \tag{A.2}$$

$$\tan\alpha = \frac{R\cos(\theta_r + \theta_s) - r}{R\sin(\theta_r + \theta_s)}. \tag{A.3}$$